Poleward microtubule flux mitotic spindles assembled in vitro

Poleward Microtubule Flux in Mitotic Spindles Assembled in Vitro

Kenneth E. Sawin and Timothy J. Mitchison

Departments of Biochemistry and Biophysics and Pharmacology, University of California at San Francisco, San Francisco, California 94143

Abstract. In the preceding paper we described pathways of mitotic spindle assembly in cell-free extracts prepared from eggs of *Xenopus laevis*. Here we demonstrate the poleward flux of microtubules in spindles assembled in vitro, using a photoactivatable fluorescein covalently coupled to tubulin and multi-channel fluorescence videomicroscopy. After local photoactivation of fluorescence by UV microbeam, we observed poleward movement of fluorescein-marked microtubules at a rate of 3 μm/min, similar to rates of chromosome movement and spindle elongation during prometaphase and anaphase. This movement could be blocked by the addition of millimolar AMP-PNP but was not affected by concentrations of vanadate up to 150 μM, suggesting that poleward flux may be driven by a microtubule motor similar to kinesin. In contrast to previous results obtained in vivo (Mitchison, T. J. 1989. *J. Cell Biol.* 109:637–652), poleward flux in vitro appears to occur independently of kinetochores or kinetochore microtubules, and therefore may be a general property of relatively stable microtubules within the spindle. We find that microtubules moving towards poles are dynamic structures, and we have estimated the average half-life of fluxing microtubules in vitro to be between ~75 and 100 s. We discuss these results with regard to the function of poleward flux in spindle movements in anaphase and prometaphase.

In recent years, the availability of molecular probes to study microtubule dynamics has provided new insights into microtubule behavior in the mitotic spindle. Photobleaching experiments have shown that microtubules turn over rapidly in the spindle (Cassimeris et al., 1988; Salmon et al., 1984*a*; Saxton et al., 1984; Wadsworth and Salmon, 1986), explaining in part its rapid response to changes in levels of microtubule polymerization (Inoue and Sato, 1967; Salmon et al., 1984*b*). Kinetochore microtubules as a class are more stable than most spindle microtubules, both in terms of turnover and resistance to depolymerizing conditions (Gorbsky and Borisy, 1989; Mitchison et al., 1986; Rieder, 1981). Different rates of microtubule turnover in the context of a relatively stable, differentiated structure such as the spindle suggest that regulation of microtubule dynamics is likely to be intimately involved in spindle morphogenesis and function (Inoue and Sato, 1967; Kirschner and Mitchison, 1986; Mitchison, 1988). By studying more carefully the behavior of microtubules in the spindle we hope to gain insights into how microtubule dynamics may be involved in spindle morphogenesis and chromosome segregation in mitosis.

It was originally demonstrated in vitro that microtubule plus ends captured by chromosomes can incorporate exogenous labeled tubulin while maintaining attachment at the kinetochore (Mitchison and Kirschner, 1985), and subsequent experiments in vivo showed that microinjected biotin-labeled tubulin incorporates into microtubule ends attached to kinetochores at metaphase (Mitchison et al., 1986). At increasing times after microinjection, kinetochore microtubules became progressively labeled from their plus ends polewards towards their minus ends. To maintain the metaphase spindle at steady-state, the progressive addition of new tubulin subunits at microtubule plus ends requires the concomitant depolymerization of microtubules at minus ends. This would result in the steady poleward movement of tubulin subunits in the microtubule lattice towards spindle poles, as was postulated by Margolis and Wilson on the basis of experiments in vitro (Margolis and Wilson, 1981). This inferred movement, which we have termed poleward microtubule flux, was recently demonstrated directly in living tissue culture cells using a novel photoactivatable fluorochrome, bis-caged fluorescein (C2CF), covalently coupled to tubulin (Mitchison, 1989). After microinjection of unactivated (non-fluorescent) C2CF-tubulin into metaphase tissue culture cells and incorporation of the tagged tubulin into spindles, fluorescence was locally activated in the spindle by UV light and followed by low-light videomicroscopy. Activated fluorescence moved polewards at a rate of 0.4–0.6 μm/min, indicating movement of the microtubule lattice. Poleward flux appeared to be specific to kinetochore microtubules; other spindle microtubules lost fluorescence rapidly, presumably because of their high rate of turnover.

The results obtained from photoactivation of fluorescence have agreed with those obtained by photobleaching methods, with respect to the rapid turnover of most spindle microtubules. However, photobleaching experiments have not detected any significant poleward movement of microtubules in

spindles (see references above), with one possible exception (Hamaguchi et al., 1987), and the reasons for this are not yet clear (see Mitchison and Sawin, 1990 and references therein). In the preceding paper we described different assembly pathways for spindles reconstituted in cell-free extracts of *Xenopus* eggs (Lohka and Maller, 1985; Murray and Kirschner, 1989; Sawin and Mitchison, 1990); in this paper we report the identification of poleward microtubule flux in spindles assembled in vitro, extending our previous observations of poleward microtubule flux. Spindles assembled in vitro provide a powerful model system for studying microtubule dynamics: they are among the largest described in higher eukaryotes (40–60 μm, pole-to-pole) and are therefore easily marked and followed by light microscopy. In addition, because they are not surrounded by a plasma membrane, spindles assembled in vitro can be subjected to a number of experimental conditions without the difficulties introduced by microinjection. The ability to manipulate this reconstituted system should allow us to pursue the mechanism of poleward flux at a biochemical level.

Materials and Methods

Extracts, Sperm, and Tubulin

The methods used for the preparation of *Xenopus* egg extracts arrested in mitosis ("mitotic extracts") or induced to enter interphase and arrested in the following mitosis ("interphase-to-mitotic extracts"), for the isolation and fluorescent labeling of *Xenopus* sperm nuclei, and for tubulin labeling have been described in the preceding paper (Sawin and Mithison, 1990). In some experiments sperm nuclei were covalently labeled with the carboxymethylindocyanine dye CY5.18, using the dye *N*-hydroxysuccinimide-ester, CY5.18-OSu (Southwick et al., 1990) and the procedure described in the previous paper. CY5.18-OSu was the generous gift of Swati Mujumdar and Alan Waggoner (Carnegie-Mellon University, Pittsburgh, PA). Bovine brain tubulin was purified and labeled with X-rhodamine and C2CF, using the dye *N*-hydroxysuccinimide- and *N*-hydroxy-sulfo-succinimide esters, respectively (Hyman et al., 1990). X-rhodamine tubulin was used in place of tetramethylrhodamine tubulin (Sawin and Mitchison, 1990) for better spectral separation from the activated C2CF (i.e., fluorescein) signal. The synthesis and properties of C2CF and C2CF-labeled tubulin have been described previously (Mitchison, 1989).

Addition of Drugs

Inhibitors, nucleotides, and nucleotide analogues were added to extracts as a 1:10 dilution of 10× solutions in sperm dilution buffer (Sawin and Mitchison, 1990). 10× solutions were made fresh from concentrated stocks. All nucleotides and nucleotide analogues were added as Mg salts. Addition of sperm dilution buffer alone had no effect on poleward flux in control experiments.

Localization of C2CF-Tubulin to Single Microtubules

For Fig. 1, *A–C*, spindles assembled in mitotic extracts in the presence of C2CF- and X-rhodamine-tubulin were spotted onto a microscope slide in the dark and photographed in both fluorescein and rhodamine channels before and after a 1-s exposure to UV light from Hoechst epi-illumination, under a Zeiss Universal fluorescence microscope with a 60X/1.4 NA objective (S Plan Apo, Olympus). For Fig. 1, *D–F*, detergent extraction of microtubule arrays into a microtubule-stabilizing buffer and centrifugation onto coverslips was performed as described previously (Sawin and Mitchison, 1990). Coverslips were mounted on microscope slides and microtubule arrays were photoactivated with UV light by a 1-s exposure to epi-illumination in the Hoechst channel. Images before and after photoactivation were acquired with a silicon-intensified target camera and recorded as 64-frame averages onto an optical memory disc recorder (OMDR, model TQ-2028F, Panasonic; Secaucus, NJ). Images were photographed from the video monitor.

Optical System

In all experiments we used a IM35 inverted microscope (Zeiss, Oberkochen, FRG) equipped with a rotating stage and 100W/12V halogen lamps for both trans- and epi-illumination; we modified the microscope for multichannel low-light fluorescence imaging, as follows. Computer-driven, shuttered filter wheels (AZI, Worcester, MA) containing optically coated, fully blocked band-pass filters (Omega Optical, Brattleboro, VT) were mounted between the epi-lamp housing and the microscope for fluorescence excitation (fluorescein, 465–495 nm; X-rhodamine, 540–580 nm) and between the microscope body and a 100/100 trinocular tube for fluorescence emission (fluorescein, 518–552 nm; X-rhodamine, 605–665 nm). Mounting the emission wheel between the microscope body and the trinoc tube increased total tube length minimally and allowed us to top-mount an intensified silicon intensified target (ISIT[1]; Cohu Inc., San Diego, CA) camera directly onto the trinocular tube without any additional optics. For fluorescein/X-rhodamine double-label fluorescence experiments, the only filter within the microscope body was a custom-designed multiple-band dichroic mirror (Omega Optical, specifications available upon request). For fluorescein/rhodamine/CY5 triple label fluorescence, the cube was slid manually between the multiple-band dichroic mirror and a 660-nm long pass dichroic; we have subsequently designed a multiple-band dichroic mirror that eliminates any movement within the microscope body. For CY5 imaging we used a 630–650-nm band pass filter and a 670-nm long pass filter for excitation and emission, respectively. This was suboptimal for CY5 fluorescence (Ernst et al., 1989) but sufficient for our purposes. The photoactivation apparatus used has been described previously in detail (Mitchison, 1989). Briefly, a UV photoactivation beam was steered into the microscope light path via a 390-nm long pass dichroic mirror in the epi-tube. The light source for photoactivation was focused on an adjustable slit conjugate to the image plane. Slit width varied among experiments but after photoactivation usually produced a fluorescent bar 3–5 μm wide at half-maximal intensity, as detected by the ISIT camera. The actual bar of activation is probably considerably narrower, but its image is broadened by high camera gain (Mitchison, 1989).

Image acquisition was controlled through a Datacube Maxvision image processor coupled to a 386 AT clone microcomputer, using home-written software (A. Hyman, K. Sawin, R. Durbin, T. Mitchison, unpublished observations). Images were collected at video rates with the ISIT camera, averaged by the image processor, and recorded with an OMDR. Frame averages were between 8 and 64 frames (0.25–2 s), depending on the experiment. At the beginning of each run, ISIT gain was manually preset to prevent saturation of the camera while maximizing dynamic range (8-bit, 256 grey-scale image); throughout each run, gain was kept constant in each channel, for subsequent quantitative image analysis. For multiple-channel observations we switched the ISIT between two preset gain settings using an external control box and a switching unit supplied by the manufacturer (Cohu). Shuttered illumination, photo-activation, filter-wheel position, ISIT camera gain switch control, and OMDR recording were all controlled by the computer through a DT2817 I/O board (Data Translation, Marlboro, MA) and home-written software.

Photoactivating and Recording Spindles

Mitotic extracts containing 0.3 mg/ml C2CF-labeled bovine brain tubulin and 0.01 mg/ml X-rhodamine-labeled bovine brain tubulin were incubated with demembranated *Xenopus* sperm nuclei at 20°C as described (Sawin and Mitchison, 1990). In some experiments sperm were prelabeled with CY5, and/or interphase-to-mitotic extracts (Sawin and Mitchison, 1990) were used in place of mitotic extracts. After spindles had formed (60–240′ after start of incubation), 4–5 μl of extract containing spindles was spotted onto a microscope slide and sealed under a coverslip with Valap (vaseline/lanolin/paraffin, 1:1:1). The slide was mounted on the microscope and spindles were identified under trans-illumination phase-contrast optics with a low magnification objective (25×/0.8 NA Neofluar, Zeiss) and a long working-distance condenser (Modulation Optics, Greenvale, NY). Phase contrast was sufficient to identify spindles in crude extracts, but inadequate for accurate position measurements, for which we relied on total spindle fluorescence in the X-rhodamine channel. After identifying spindles, the objective was switched to 100× (1.4 NA Neofluar, Zeiss) and spindles were aligned orthogonal to the axis of the photoactivation slit. An image acquisition sequence was begun, recording both (or all three) fluorescent channels

1. *Abbreviation used in this paper*: ISIT, intensified silicon-intensified target.

at 5–30-s intervals, depending on the experiment; different channels were separated by a lag of ~1-3 s, depending on how many frames were averaged in each channel. After preactivation images had been collected, spindles were photoactivated for 2–4 s (Mitchison, 1989), without interrupting the recording sequence, which was continued until photoactivated fluorescence was no longer detectable. Sometimes we activated the same spindle multiple times in the same sequence without any deleterious effects. Except where noted, epi-fluorescence illumination was shuttered during all experiments, although this turned out not to be necessary (see Results). When experiments were done without shuttered illumination in order to test for possible photobleaching due to observation, samples were illuminated between frame acquisition in the fluorescein channel. Throughout experiments the temperature of the microscope stage was kept constant at 20 ± 1°C.

Image Analysis

Images played back on the OMDR were digitized using either JAVA (Jandel Scientific, Corte Madera, CA) or Image-1 (Universal Imaging Corp., West Chester, PA) software. Fluorescence profiles of photoactivated marks were generated at successive time points in the following manner: while observing total spindle fluorescence (in the X-rhodamine channel), a rectangular region whose long axis was parallel to the spindle axis was marked on the video screen with a mouse, and the average fluorescence intensity per line of pixels normal to the spindle axis was recorded along the length of the rectangle in both fluorescein and X-rhodamine channels, and in the CY5 channel where indicated. The number of pixels averaged for each point (i.e., the height of the rectangle) varied between 15 and 50, depending on the spindle being analyzed; we have found empirically that increasing the number of pixels averaged beyond 10 affects only the smoothness of the profiles obtained. To observe changes in fluorescence intensity profiles quickly and interactively when initial image intensities were well below saturation, we usually enhanced the contrast of the fluorescein signal before digitization, using digital contrast enhancement software. This is a strictly linear transformation and was performed in the same manner on all images analyzed in a particular sequence. Digitized data were transferred to a spreadsheet program (Excel; Microsoft, Redmond, WA) and plotted, after subtracting the intensity profile of a digitized preactivation fluorescein image from each analyzed image. Zero time points shown in the figures represent the first recorded frame after photoactivation, which was usually 2–4 s before. Spreadsheet tables were then used to determine peaks of fluorescence profiles nonsubjectively, and rates of flux were calculated as movement of fluorescence peaks over time. Using these methods, X-rhodamine fluorescence profiles were superimposable throughout sequences, indicating that regions being analyzed had remained stationary with respect to total spindle fluorescence.

Spreadsheet values for fluorescence intensity were also used to estimate the rate of fluorescence loss after photoactivation, by plotting peak fluorescence over time. We consider peak fluorescence to be a better indicator than integrating total spindle fluorescence because of nonlinearities in ISIT response and camera bloom at the gain and contrast settings used. We calibrated the ISIT camera at a number of different intensities and gain settings and found response to be strictly linear only within a narrow range of intensities, with small but measurable variation across the camera face plate (not shown). This in no way affects our conclusions concerning the phenomenon of poleward flux, which require measurements of only relative fluorescence intensities that can be normalized to X-rhodamine fluorescence. However, slight ISIT nonlinearities do affect our ability to accurately determine rates of microtubule turnover, which are presented in uncorrected form because of the uncertainties involved in correction. We address this further in the Results section.

Three-color Image Superposition (Fig. 6).

To generate three-channel color images from successive (i.e., fluorescein, X-rhodamine, and CY5) video frames at the same time point, we digitally compressed successive eight bit (256 grey-scale) images to two three bit images (fluorescein and X-rhodamine) and one two bit image (CY5) using home-written software. These were then combined into a composite 8-bit image in which the three most significant bits represented information from the fluorescein image, the three middle bits data from X-rhodamine, and the two least significant bits CY5. This composite image was then expanded into a three-color image by an appropriate modification of the red, green, and blue output look-up tables of the image processor and photographed from the video monitor. The contrast of such an image is rather reduced from the original images, in part because of data compression and in part because of color blending. However, color video sequences created by these methods demonstrate poleward movements in a manner that is not as readily apparent in monochrome videos (not shown).

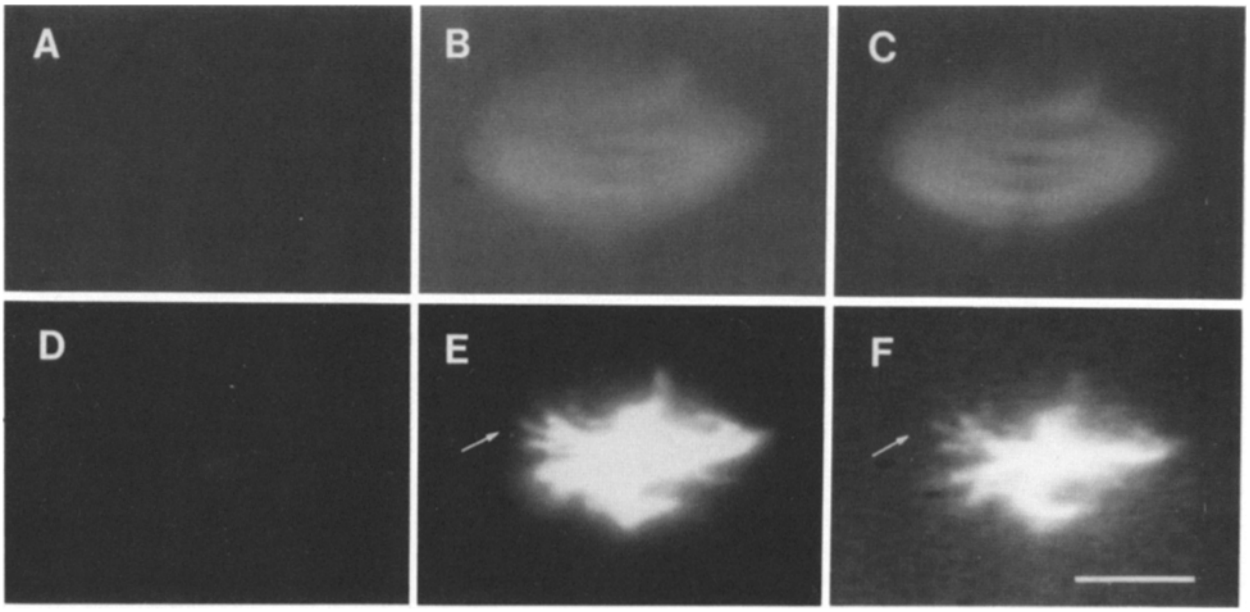

Figure 1. Incorporation of C2CF-labeled tubulin into spindle microtubules in *Xenopus* egg extracts. (*A–C*) Assembled spindle and (*D–F*) small astral array after incubation with X-rhodamine-tubulin and C2CF-tubulin. (*A* and *D*) Fluorescein signal before UV photoactivation; (*B* and *E*) fluorescein signal after 1 s exposure to UY epi-illumination; (*C* and *F*) X-rhodamine signal, before UV illumination. Arrows indicate single microtubules in *E* and *F*. Fluorescein images before and after photoactivation were photographed and printed under identical conditions. Bar: (*A–C*) 10 μm; (*D–F*) 3 μm.

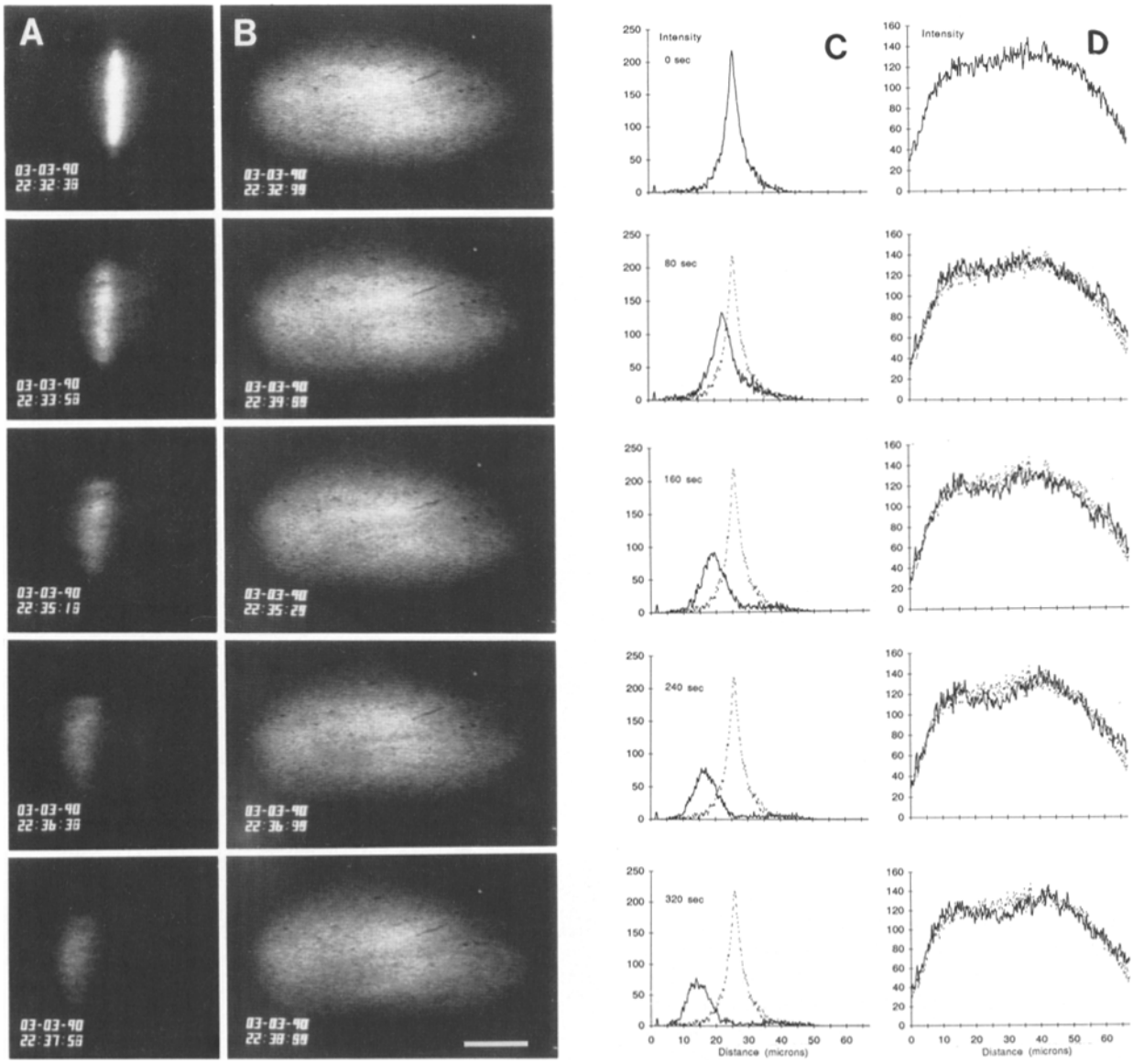

Figure 2. Poleward microtubule flux in spindles assembled in vitro. ISIT camera images of (*A*) photoactivated fluorescein and (*B*) X-rhodamine signals in a spindle at increasing times after photoactivation: 0, 80, 160, 240, and 320 s. Images are 64 video-frame (i.e., 2 s) averages, so the hours:minutes:seconds clock signals appear abnormal in some places. (*C* and *D*) Digitization of fluorescein and X-rhodamine fluorescein, matching frames of *A* and *B*, respectively, prepared as described in Materials and Methods. Fluorescence intensity at indicated times (*solid lines*) is superimposed on fluorescence intensity at time zero (*dashed lines*). Ordinate is intensity (arbitrary units), abscissa is distance across the spindle, in microns. Note the steady poleward movement of fluorescence and decay in fluorescein signal over time, while the rhodamine signal remains essentially unchanged.

Results

C2CF-Tubulin Incorporation into Spindle Microtubules In Vitro

We have previously described the poleward flux of microtubules in metaphase spindles in vivo, using a novel photoactivatable compound, bis-caged fluorescein (C2CF) covalently coupled to tubulin (Mitchison, 1989). We were interested in knowing whether metaphase spindles assembled in *Xenopus* oocyte extracts in vitro (Sawin and Mitchison, 1990) would show the same type of behavior. To test whether C2CF-labeled tubulin would faithfully incorporate into extract spindle microtubules, we added X-rhodamine-labeled bovine brain tubulin (0.01–0.015 mg/ml) and C2CF-labeled brain tubulin (0.3 mg/ml) to mitotic egg extracts and incubated them with demembranated *Xenopus* sperm nuclei. Morphologically normal spindles assembled in the extracts and were visible in the rhodamine channel but not in the fluorescein channel before photoactivation, as shown in Fig.

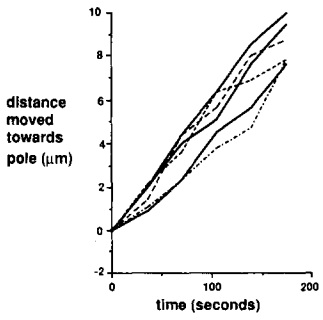

Figure 3. Rate of poleward flux in spindles in vitro. Distance moved towards pole over time, from six independent runs; average rate is 2.9 ± 0.4 (SD) μm/min. Distance at time points determined as described in Materials and Methods, from position of peaks in fluorescence profiles like those of Fig. 2.

1, *A* and *C*. A fluorescein signal identical with rhodamine fluorescence arose after a 1-s exposure to UV epi-illumination (Fig. 1 *B*), indicating that C2CF-labeled tubulin had incorporated into spindle microtubules. To confirm that photoactivated fluorescence was on single microtubules, we diluted microtubule arrays assembled in extracts into a microtubule stabilizing buffer, extracted them with Triton X-100, and centrifuged them onto coverslips under safe-light conditions. Essentially no fluorescein signal was visible until photoactivation by UV epi-illumination (Fig. 1 *D*), after which fluorescein and rhodamine fluorescence were coextensive (Fig. 1, *E* and *F*). Photoactivatable tubulin in microtubule arrays is therefore not detergent extractable. After detergent extraction, what are probably single microtubules could be seen protruding from photoactivated microtubule bundles (Fig. 1, *E* and *F*, *arrows*).

Poleward Microtubule Flux

Spindles assembled in vitro in the presence of C2CF- and X-rhodamine-tubulin were locally irradiated for 2–4 s by a 360-nm UV microbeam introduced into the microscope. We followed the disposition of locally activated fluorescence at increasing times after photoactivation with a computer-controlled videomicroscope and digital image processing (Materials and Methods). Because the phase-contrast images obtainable from crude oocyte extracts are usually of low quality (Sawin and Mitchison, 1990) we tracked the spindle by X-rhodamine fluorescence, so that movements of the photoactivated fluorescent bar could be normalized to possible changes in spindle fluorescence or position. Fig. 2, *A* and *B* show that under conditions where spindles were stationary, the fluorescein signal moved towards the pole over time, as a single moving phase, which we interpret as poleward movement of the microtubule lattice (Mitchison, 1989). During this poleward movement there is a continuous decrease in fluorescein intensity, the reasons for which are investigated further below. To demonstrate poleward movement of microtubules more quantitatively, we measured fluorescein and rhodamine intensities throughout spindles at successive time intervals. Analysis of video sequences also showed that photoactivated fluorescence in spindles moved poleward as a single peak. In addition, while total photoactivated fluorescence decreased in intensity over time, as peaks moved poleward the absolute intensity of fluorescence near the pole specifically increased, as shown in the sequence in Fig. 2 *C*. This indicates that the movement of fluorescence perceived by eye in recorded video sequences represents actual movement of fluorescence and not a more complex anisotropic loss of photoactivated fluorescence within the spindle. Throughout sequences, the intensity and position of (control) X-rhodamine fluorescence was essentially unchanged (Fig. 2 *D*). These results quantitatively demonstrate that fixed points on the microtubule lattice move steadily poleward, while spindle length remains constant. We refer to this phenomenon as poleward microtubule flux.

Rate of Poleward Flux

We determined the rate of poleward microtubule flux by plotting the position of quantitated fluorescence peaks at successive time intervals after photoactivation. Measurements obtained by this method were within 10% of rates determined by simple but more subjective measurements directly from the video monitor. Rates determined by either method were found to be between 2.5 and 3 μm/min, in over 50 experiments. As shown in Fig. 3, movement is essentially linear over time. The average rate from several independent runs was 2.9 ± 0.4 (SD) μm/min, and average values fit a least-squares linear regression rather well ($r^2 > 0.999$). It is difficult to attach any specific error to measurements of flux rates, because of the decrease in signal intensity and gradual spreading of fluorescence profiles after photoactivation, especially at later times.

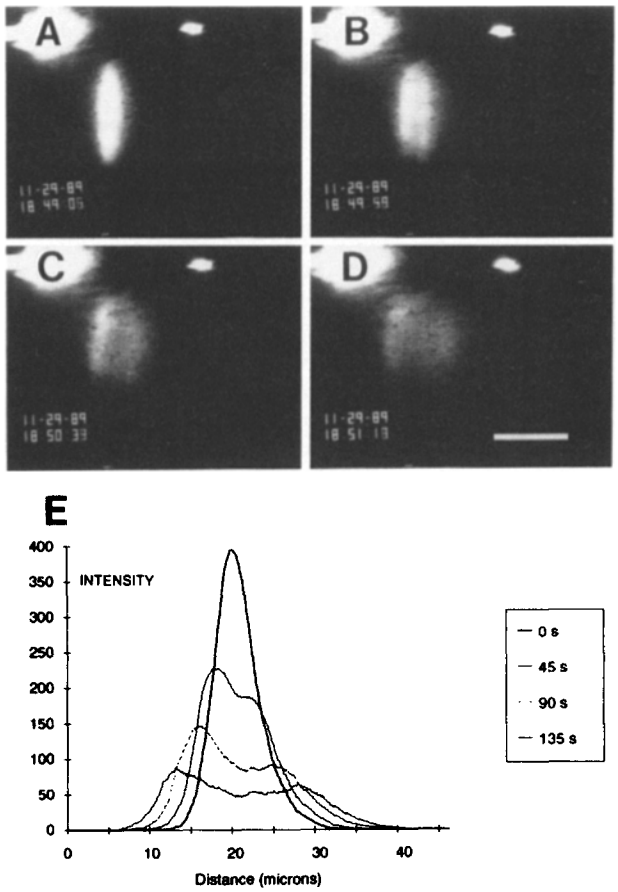

Figure 4. Bar-splitting after photoactivation in the central spindle. Spindle was activated centrally, as determined by X-rhodamine fluorescence (not shown). (*A–D*) ISIT camera images of photoactivated fluorescence at increasing times after activation; (*A*) 0, (*B*) 45, (*C*) 90, and (*D*) 135 s. (*E*) Digitization of the same frames shown in *A–D*. X-rhodamine fluorescence remained stationary (not shown). Bar, 20 μm.

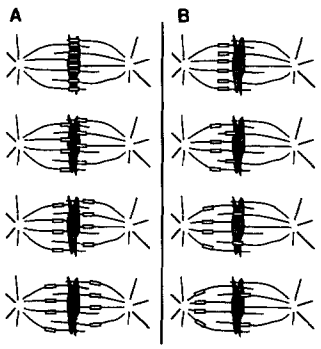

Figure 5. Interpretation of bar-splitting after photoactivation in the central spindle. (*A*) Local activation of fluorescence in the spindle center. Lines are microtubules, stippled regions are chromatin, and white bars are photoactivated segments of microtubules. After photoactivation (*lower panels*), fluorescence splits equally in each direction, because microtubules from each half of the spindle contribute equally to microtubule density at the site of activation. However, because chromatin is also in the spindle center, the role of kinetochores and/or chromatin in poleward flux remains unclear. (*B*) Eccentric photoactivation. Fluorescence splits asymmetrically, and a small portion of fluorescence moves through the chromatin towards the distal spindle pole.

Simultaneous Poleward Flux in Each Half of the Spindle

In many photoactivation runs we noticed that a small fraction of total fluorescence seemed to move away from the pole rather than towards it, while essentially no fluorescence remained stationary. We investigated this further by photoactivating marks at different points in the spindle. Fluorescent marks generated in the center of the spindle split equally into two marks that moved in opposite directions, each at ~3 μm/min, as shown in Fig. 4. Interestingly, when spindles were marked slightly off-center, the majority of fluorescence in such "bar-splitting" events always moved towards the proximal (near) pole. In addition, the fraction of total fluorescence moving towards this pole increased as marks were made closer to it. We have previously shown that half-spindles can form autonomously in egg extracts, and fuse together to form essentially the two halves of the spindle (Sawin and Mitchison, 1990). We interpret bar-splitting as simultaneous poleward microtubule flux in each of the two halves of the spindle, seen most clearly in the spindle midzone, where microtubules of opposite polarity overlap. This implies that flux in a single direction represents poleward movement of microtubules of identical polarity, emanating from the same spindle pole, as diagrammed in Fig. 5 *A*. Bar-splitting was not observed in our original experiments on polewards microtubule flux in vivo (Mitchison, 1989); this may reflect increased central spindle microtubule bundling and/or overlap in *Xenopus* egg extract spindles assembled in vitro (Sawin and Mitchison, 1990) compared to tissue culture cell spindles.

Poleward Flux Is Not Specific to Kinetochore Microtubules

Because the bulk of mitotic chromatin is in the central spindle, where bar-splitting was most prominent, we next investigated the role of chromatin and kinetochores in poleward microtubule flux. Our previous experiments in vivo (Mitchison, 1989) detected flux exclusively in what appeared to be kinetochore microtubules (Mitchison et al., 1986). However, because spindles assembled in mitotic extracts in vitro do not contain kinetochores identifiable by EM morphology (Sawin and Mitchison, 1990), we wondered if poleward flux in spindles assembled in vitro might not be specific to microtubules terminating in chromatin (e.g., kinetochore microtubules). We therefore designed an experiment to follow the fate of photoactivated microtubules that extend be-

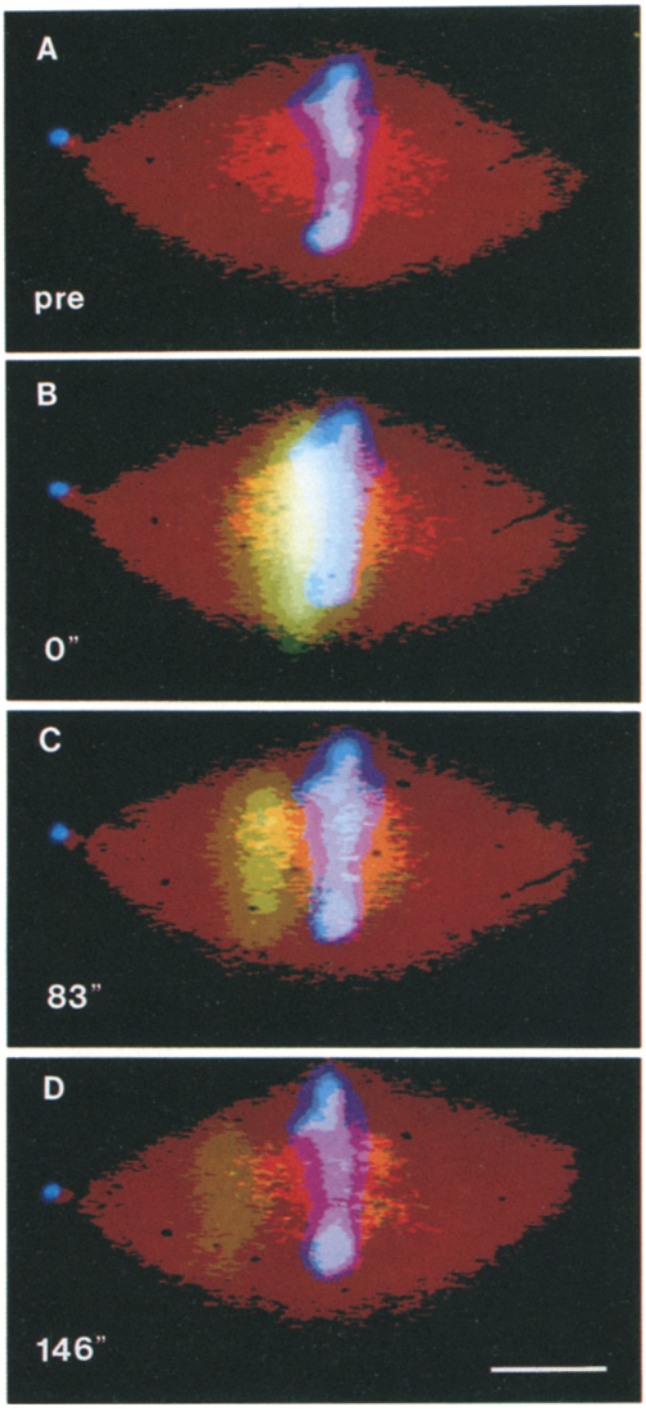

Figure 6. Bar-splitting and microtubule flux towards the distal pole. Triple-label marking experiment. (*A–D*) Three-color image of spindle, generated by superimposing ISIT images digitally, as described in Materials and Methods. Times after photoactivation are given in seconds, and do not correspond exactly to the plots shown in Fig. 7. Image has reduced contrast, because of data compression and color blending (see Materials and Methods). Bar, 10 μm.

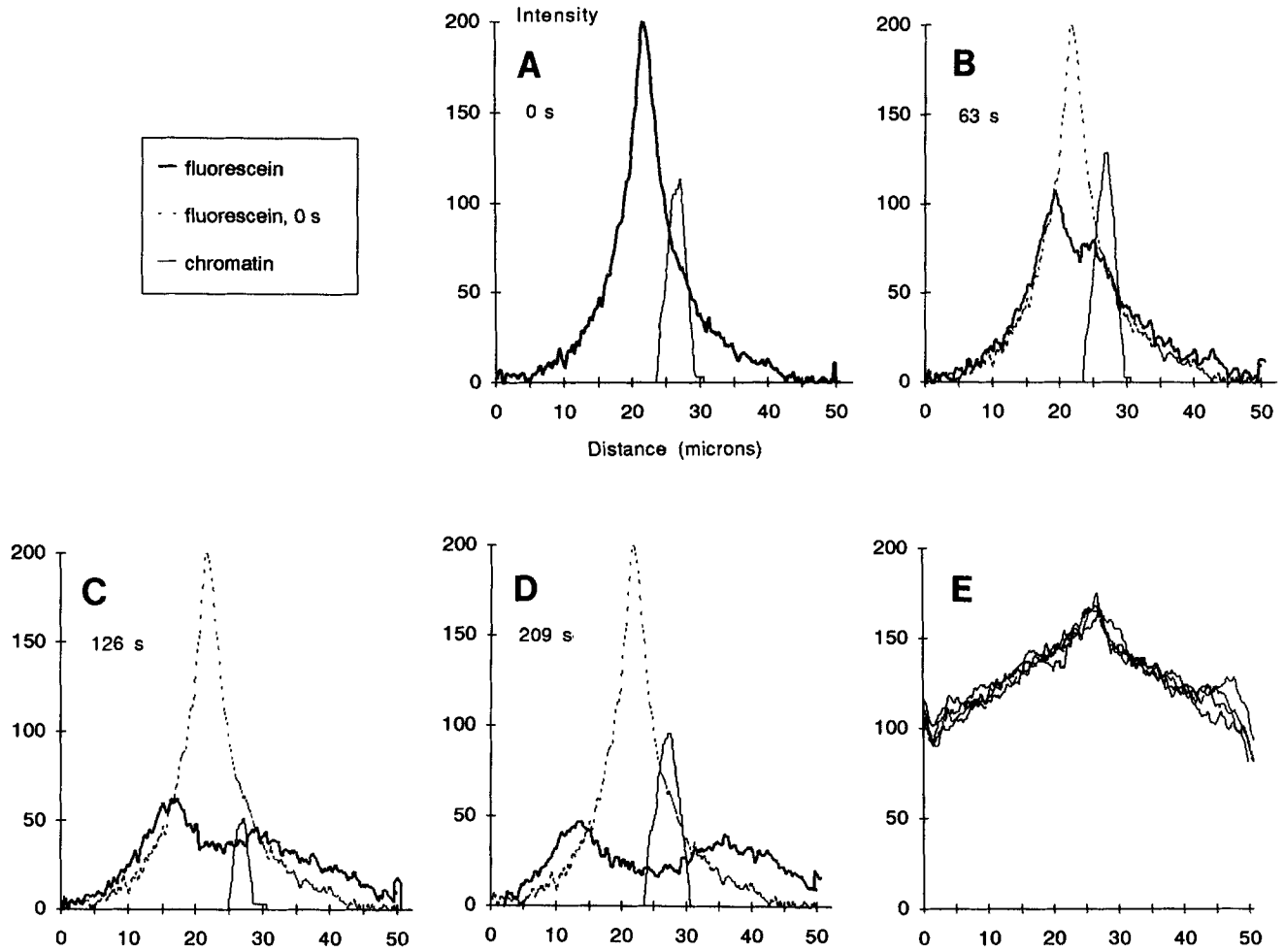

Figure 7. Bar-splitting and microtubule flux towards the distal pole. Digitizations of (*A–D*) fluorescein-tubulin and CY5-chromatin, and (*E*) X-rhodamine-tubulin fluorescence intensities after eccentric photoactivation in the central spindle, for the spindle shown in Fig. 6. (*A–D*) Fluorescence intensity profiles through the spindle at increasing times after photoactivation (*dark solid lines*), given in seconds, superimposed on the profile from time zero (*dashed lines*). The CY5 signal at the same times is also shown (*light solid lines*). Lamp flicker at 126 s caused a reduced signal in the CY5 channel only; this was obvious by eye. ISIT camera bloom from brightness of chromatin results in relatively wide peak (~4 μm at half-maximal intensity), actual chromatin is narrower (Sawin and Mitchison, 1990). (*E*) X-rhodamine fluorescence intensity profiles, superimposed for all of the times shown in *A–D*. The peak in *E* represents bleed-through of CY5 into the rhodamine channel and marks the spindle center. Note that photoactivated fluorescence can be seen heading towards chromatin in *B*, and continues to move through chromatin towards the distal pole in *C* and *D*, while both chromatin and total spindle fluorescence remain stationary.

yond chromatin, from one half-spindle into the opposing half-spindle. This necessitated visualizing chromatin during observations of microtubule flux. To identify chromatin in spindles we modified the microscope system to record three fluorescent channels simultaneously and prelabeled sperm nuclei with the far-red fluorescent dye CY5.18 (Southwick et al., 1990). Although we were able to observe chromatin by UV-Hoechst staining, CY5 labeling of chromatin was necessary because 360-nm light photoactivates C2CF.

Fluorescence was locally activated in the spindle midzone, sufficiently close to the center to observe bar splitting but far enough from chromatin to resolve photoactivated tubulin fluorescence from the CY5 signal. In these triple-labeled marking experiments we observed bar-splitting, i.e., flux towards both proximal and distal poles, under conditions where both spindles and chromatin remained stationary. To illustrate this phenomenon more clearly we have digitally superimposed, in pseudocolor, the three separate monochrome channels from one such sequence, shown in Fig. 6. Flux towards the distal pole is not as obvious in this figure as in monochrome images (not shown), since the gray-scale and contrast of monochrome images had to be significantly compressed before superposition. However, upon digitization and superposition of fluorescence profiles from the original monochrome data, it is clear that photoactivated fluorescence splits and moves in both directions, as is shown in Fig. 7, *A–E*. We further note in the evaluation of these data, that while in Fig. 7 *A* there is already activated fluorescence to the right of and "underneath" chromatin at time zero (because of beam spread and camera bloom), a simple analysis based on loss of fluorescence from microtubule turnover (see below) indicates that this fraction of fluorescence cannot quantitatively account for all of the fluorescence exclusively to the right of chromatin in Fig. 7 *D*. We therefore conclude that photoactivated fluorescence does indeed move through chromatin towards the distal pole.

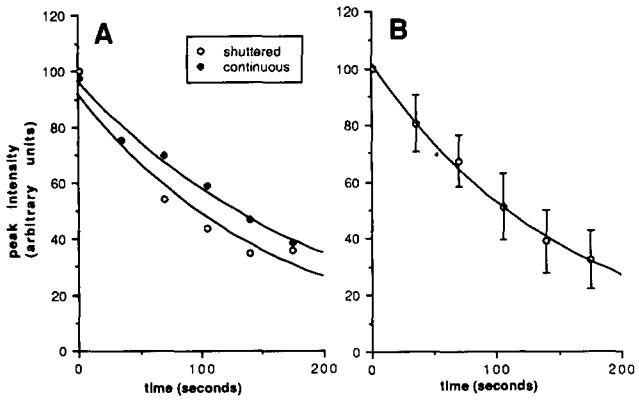

Figure 8. Demonstration of the absence of photobleaching and measurement of microtubule turnover after photoactivation. (*A*) Decay of peak fluorescence in a spindle first activated and followed with shuttered illumination (*open circles*) and then reactivated and followed with continuous illumination (*closed diamonds*) under identical conditions. Spindles followed under continuous illumination received 10–20 times the irradiance of spindles followed under shuttered illumination. (*B*) Average of fluorescence decay for six independent runs with different spindles. Average peak intensity, normalized to 100 at time zero. Error bars are SD. Data are from the same fluorescence profiles used to determine rate of poleward flux in Fig. 3.

On the basis of our interpretations of bar-splitting, this movement indicates that microtubules whose plus ends are distal to (i.e., not terminating in) chromatin are capable of fluxing through chromatin towards their respective spindle poles, as shown in Fig. 5 *B*. Conventionally, kinetochore microtubules are defined as having their plus ends terminating in chromatin. In conjunction with the absence of kinetochores in spindles assembled in mitotic extracts, these results indicate that kinetochore fibers are not required for poleward microtubule flux. Rather, they suggest that poleward flux may be a more general property of microtubules within the spindle.

Microtubule Turnover during Poleward Flux

In most experiments we were unable to follow the movement of photoactivated fluorescence for long periods of time, since the fluorescein signal decreased rapidly in intensity and was usually no longer detectable after a few minutes. We therefore wanted to determine whether this was due primarily to photobleaching or to turnover of fluxing microtubules. To determine more quantitatively the extent of photobleaching we photoactivated spindles and observed fluorescence over time under widely varying conditions of illumination. We first photoactivated and followed fluorescence with shuttered illumination; we then reactivated the same spindle and followed fluorescence under continuous illumination at 490 nm, to maximize potential photobleaching in the fluorescein channel. By photoactivating the same spindle twice, experiments were internally controlled; we have found that fluorescence can be photoactivated repeatedly in spindles without any effects on poleward flux, and that spindles can be observed for long periods of time at 490 nm without any consequent activation of fluorescence (data not shown). Images of photoactivated fluorescence under the two different conditions of shuttered and continuous illumination were nearly identical at similar time intervals in a number of experiments. To quantitate this, we plotted peak fluorescence against time from sequences of the same spindle under the two conditions. Fig. 8 *A* shows the similarity of fluorescence decay curves for a spindle first photoactivated and followed with shuttered illumination and then reactivated and followed with continuous illumination. We estimate that under conditions of continuous illumination, spindles were exposed to a total irradiance 10–20 times that of shuttered illumination. Because signal loss is independent of irradiance, we conclude that the loss in fluorescence intensity in spindles observed after photoactivation results exclusively from microtubule turnover. We further note that the identical appearance of spindles under continuous and shuttered illumination later times after photoactivation indicates that the illumination used in our experiments does not significantly affect spindle organization.

The absence of photobleaching in our experiments allowed us to estimate rates of microtubule turnover in spindles. Fig. 8 *B* shows the peak intensity of quantitated fluorescence plotted against time for the six experiments shown in Fig. 3, after normalizing to unity at time zero. Fluorescence loss followed a monotonic decay that could be fit to a single exponential, with a half-life of ~100 s. Because of nonlinearities in the ISIT camera (see Materials and Methods), we emphasize that this is only a rough estimate of microtubule turnover, and we cannot exclude the possibility of a small population of microtubules that are more or less stable than the bulk population. Nevertheless, calibration of the ISIT camera as it was used in these experiments suggests that a half-life of 100 s is accurate to within at least a factor of two but probably a slight overestimate; we therefore consider an average half-life of 75–100 s to be a reasonable estimate of microtubule half-life.

Table I. Effects of Nucleotide Analogues on Spindle Stability and Poleward Flux

Reagent*		Spindle stability‡	Flux
ATP	1 (mM)	++	+
	10	–	
ATP-γ-S	1	++	+
	10	–	
AMP-PNP	0.2	++	+
	0.5	+	ND
	1.7	+	–
	5	–	
GTP	1	++	ND
GTP-γ-S	1	++	ND
MgCl2 (control)	1	++	+
	10	–	
Vanadate	50 (μM)	+	+
	150	+	+
	500	–	
no ATP-RS§	–	++	+
no ATP-RS + Vanadate	170 (μM)	+	+

* All nucleotides added as magnesium salts; vanadate heated before use.
‡ ++, No effect on spindle stability; +, varying effects; eventual but slow spindle dissolution; –, rapid spindle dissolution, flux experiments impossible under these conditions.
§ No ATP-regenerating system; see Materials and Methods.

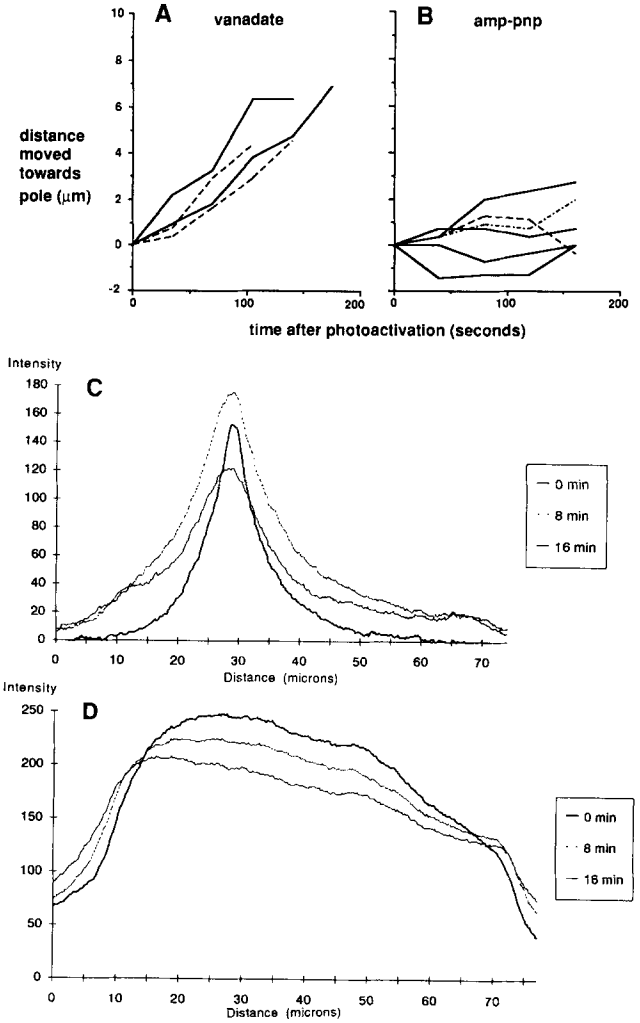

Figure 9. Effects of nucleotide analogues on poleward microtubule flux. (*A*) Poleward flux is not significantly affected by 50 mM (*dashed lines*) or 150 mM (*solid lines*) vanadate. Rate of movement appears to be slightly reduced vs. controls, but comparable at both concentrations of vanadate. (*B*) Inhibition of poleward flux by 1.7 mM AMP-PNP. Qualitatively, flux is completely blocked. Methods follow those in Fig. 3. (*C* and *D*) Effects of AMP-PNP on microtubule turnover. (*C*) Fluorescein intensity profiles in a spindle at different times after photoactivation in the presence of AMP-PNP. Peak fluorescence intensity occasionally rises slightly over time, for unknown reasons, and then decays slowly. (*D*) X-rhodamine intensity in the same spindle at the same times. Fluorescence slowly declines, without the comparable rise shown in *C*. Decline in fluorescence is presumably due to effects of AMP-PNP on spindle stability.

Poleward Flux Is Inhibited by AMP-PNP but Not by Vanadate

We have previously hypothesized that poleward flux may be driven by a microtubule-based motor (Mitchison et al., 1986; Mitchison, 1989; Mitchison and Sawin, 1990). We therefore tested the sensitivity of poleward flux to inhibitors of microtubule motors by adding nucleotide analogues to spindles already assembled in extracts. Results from these experiments are summarized in Table I. Inhibitors had pleiotropic effects on spindle and chromatin morphology in crude mitotic extracts, ranging from small changes in spindle organization (e.g., 0.5 mM AMP-PNP) to spindle disruption and eventual conversion to an interphase-like state (e.g., 150 μM vanadate). Because of these effects, flux measurements were made within 5–10 min after inhibitors were added to spindles, before any obvious structural changes had occurred. Effects on spindle stability were not always accompanied by similar effects on poleward flux; for example, 150 μM vanadate slowly disrupted spindle morphology but showed little or no effects on the rate of flux while measurements could still be made. In the presence of vanadate, flux rates were perhaps slightly lower than those seen in control experiments but approximately the same at both 50 and 150 μM vanadate (Fig. 9 *A*).

In contrast, AMP-PNP could inhibit poleward flux completely (Fig. 9 *B*) while only slightly altering spindle organization. The effects of AMP-PNP were dose-dependent; 0.2 mM AMP-PNP had not effect on poleward flux or spindle stability, while 5 mM AMP-PNP rapidly disrupted spindles. 1.7 mM AMP-PNP inhibited poleward flux and often induced the formation of microtubule bundles within spindles before spindles eventually dissolved (data not shown). Interestingly, when 1.7 mM AMP-PNP was added to spindles we often noticed an abnormal stabilization of fluorescence after photoactivation (Fig. 9, *C* and *D*), which we attribute to a specific decrease in microtubule turnover, perhaps as a

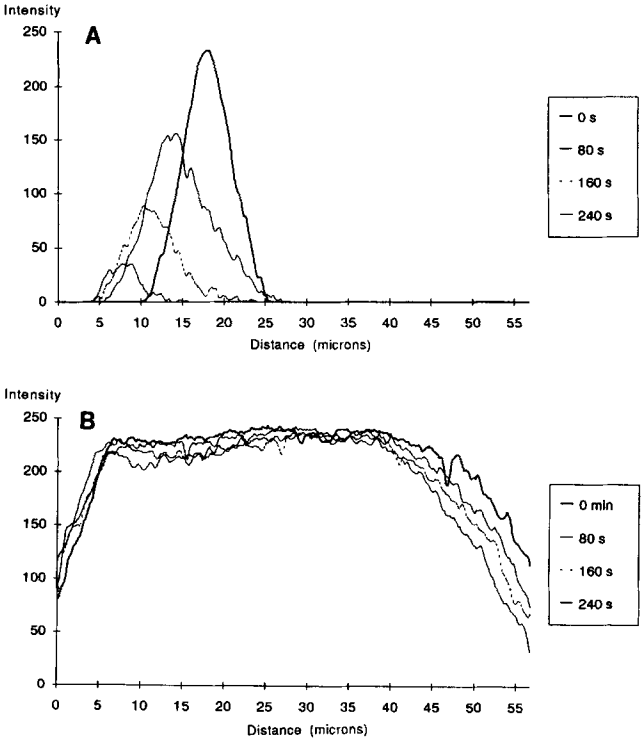

Figure 10. Microtubule flux in spindles assembled by an alternate pathway. (*A*) Fluorescein intensity profiles at increasing times after photoactivation. (*B*) X-rhodamine signal at same times. Spindle was assembled in an interphase-to-mitotic extract, as described in Materials and Methods. Note that the rate of poleward flux and the rate of fluorescence decay are nearly identical to those of spindles assembled in mitotic extracts. The shape of fluorescence profiles over time is primarily a function of the original profile at time zero and was not significantly different between mitotic extracts and interphase-to-mitotic extracts.

consequence of bundling. This stabilization also confirms the conclusion that no significant photobleaching occurs in our experiments. From these experiments we estimate microtubule half-life to be increased from ~100 s to over 15 min in the presence of AMP-PNP. In some experiments this stabilizing effect was less pronounced, although flux was still quantitatively blocked; the reasons for this variation are not yet understood, but may reflect differences in amounts of endogenous competing ATP in extracts. We never observed any similar stabilization in control experiments. We did not notice any striking effects of vanadate on microtubule turnover in a similar analysis, although many sequences indicated that turnover might be slightly increased in the presence of vanadate (data not shown).

As shown in Table I, most inhibitors had no effects on poleward flux, while high concentrations of both inhibitors and control treatments (e.g., ATP or MgCl2 alone) disrupted spindle organization too rapidly for flux measurements to be made. As a result, only in the case of AMP-PNP were we able to establish even a rudimentary dose-response relationship. We note, however, that the relative sensitivities of poleward flux to AMP-PNP and vanadate are similar to those of kinesin, a well-characterized plus-end directed microtubule motor (Cohn et al., 1989; Vale, 1987), and unlike those of cytoplasmic dynein, a minus-end directed motor (Paschal and Vallee, 1987; Shpetner et al., 1988).

Poleward Flux in Spindles Assembled by a Different Pathway

In the preceding paper (Sawin and Mitchison, 1990) we demonstrated that demembranated sperm nuclei can assemble mitotic spindles in *Xenopus* oocyte extracts by two different pathways, depending on whether they are added directly to extracts arrested in mitosis ("mitotic extracts") or allowed to form interphase nuclei before entering and arresting in mitosis ("interphase-to-mitotic extracts"). Although our data suggest that the same fundamental molecular mechanisms are responsible for spindle assembly in both pathways, we were concerned that poleward flux might be specific to spindles assembled in mitotic extracts. We therefore performed analogous flux experiments on spindles assembled in extracts that were induced to enter interphase and then driven into mitosis by the further addition of mitotic extract (Sawin and Mitchison, 1990). Qualitative observations of poleward flux in spindles assembled in interphase-to-mitotic extracts were indistinguishable from flux seen in spindles assembled in mitotic extracts. Similar results were obtained upon quantitative analysis of fluorescence, as shown in Fig. 10. We also observed bar splitting in these spindles, and this could be quantitated (data not shown). Poleward microtubule flux is therefore not an artifact of the particular pathway of spindle assembly used in our experiments.

Discussion

Poleward Movement of Fluorescence

Poleward movement of microtubules in the metaphase spindle was first inferred from EM studies of incorporation of biotinylated tubulin into kinetochore fibers (Mitchison et al., 1986), and in subsequent studies poleward microtubule flux was demonstrated directly, using a novel photoactivatable fluorochrome (C2CF) coupled to tubulin (Mitchison, 1989). Here we have demonstrated microtubule flux in spindles assembled in vitro, using fluorescence analogue cytochemistry and multi-channel fluorescence videomicroscopy. Poleward microtubule flux occurs at similar rates in spindles assembled by either of two pathways in vitro, and by studying poleward flux in vitro we have uncovered aspects of flux previously unobserved in vivo. Further work in this model system should help us to understand both the biochemical basis for poleward flux and its function and regulation during mitosis.

The demonstration of poleward movement of microtubules requires first that C2CF-tubulin incorporate faithfully into spindle microtubules and, second, that one can document true poleward movement of fluorescence after photoactivation. A number of lines of evidence indicate that C2CF-tubulin incorporates normally into spindles assembled in vitro: Photoactivation of entire spindles produces a fluorescein image that is coextensive with rhodamine-tubulin fluorescence, which is in turn coextensive with anti-tubulin immunofluorescence in spindles (data not shown; Sawin and Mitchison, 1990). Furthermore, microtubule arrays assembled in extracts containing C2CF-tubulin are still photoactivatable after detergent extraction, and single photoactivated microtubules can be observed in these arrays. Single microtubules assembled from pure C2CF-tubulin are also photoactivatable in vitro, as shown in previous work (Mitchison, 1989). We note that alternatives to C2CF-tubulin incorporation into spindle microtubules are themselves highly improbable. Localization of C2CF-tubulin to a vesicular compartment would make photoactivation of fluorescence detergent-extractable, which is not the case. If, on the other hand, photoactivatable fluorescence were localized to a detergent-insoluble particle, one would need to explain how these particles could be photoactivatable when spindle microtubules are not, as photoactivated fluorescence moves as a single phase without any stationary fluorescent "residue," and fluorescence decreases over time without photobleaching, consistent with microtubule turnover. We consider it unlikely that photoactivation itself might generate microtubule fragments or particles by the local disruption of microtubules (Vigers et al., 1988). The limited illumination used in our experiments has no significant effects on the structure of single microtubules in vitro (Michison, 1989), and in the experiments described here, the same spindle can be photoactivated at least up to six times without any deleterious effects on poleward flux or spindle structure.

We have also shown, by quantitative image analysis, that photoactivated fluorescence increases near spindle poles with time, while decreasing at the initial site of activation. If dynamically unstable microtubules (Mitchison and Kirschner, 1984; Walker et al., 1988) were to rescue anisotropically in the spindle mid-zone after initiating shrinking ("tempered instability"; Sammak et al., 1987), fluorescence might conceivably appear to move towards the pole over time. However, fluorescence would never be expected specifically to increase in any part of the spindle, while we have shown that this occurs under a number of different conditions (see, for example, Figs. 2, 7, 10). The poleward movement perceived by eye in our experiments therefore represents true movement of fluorescence within the spindle. In summary,

we conclude that the movement of fluorescence observed in our experiments reflects the steady poleward flux of the microtubule lattice.

Microtubule Flux without Kinetochores

The observation of bar-splitting in spindles in vitro suggested that poleward flux in spindles assembled in vitro might not be specific to kinetochore microtubules. C2CF-tubulin photoactivation experiments (Mitchison, 1989) were originally motivated by fixed time-point microinjection studies indicating that microtubule plus ends attached to kinetochores could nevertheless incorporate tubulin dimer during metaphase (Mitchison et al., 1986). While these experiments in vivo are consistent with poleward flux occurring primarily, if not exclusively, in kinetochore microtubules, we have failed to identify morphological kinetochores or kinetochore microtubules in spindles assembled directly from sperm nuclei in mitotic egg extracts (Sawin and Mitchison, 1990). Could the observation of poleward flux be taken as evidence that kinetochores or kinetochore microtubules are present in spindles even when we fail to detect them? We consider this unlikely; on the contrary, three independent lines of evidence suggest that microtubule flux is not directly dependent on kinetochores or chromatin. First, in spindles that lack kinetochores, poleward flux is essentially indistinguishable from flux in spindles that contain kinetochores. This implies that neither the presence nor absence of kinetochores has a significant effect on poleward flux. Second, we note that on a few occasions, we have observed aberrant spindles in which poleward flux moves as a single uniform front across the entire width of the spindle, whereas the chromatin is actually off to one side (data not shown). Because such spindles are rare, we have not analyzed this any further, but this result strongly suggests that flux does not require the direct participation of chromatin. Finally, in more reproducible triple-label marking experiments, we have shown that microtubules can flux through chromatin towards the distal spindle pole. Based on our interpretation of microtubule polarity from bar splitting, this indicates that microtubule plus ends do not need to terminate in chromatin in order to flux polewards. That is, even if kinetochores were present in chromatin, they could not be required for poleward microtubule flux. Formally, we cannot rule out the possibility that kinetochore-like structures unattached to chromatin are present diffuse throughout the cytoplasm, but we have no way of detecting them (Sawin and Mitchison, 1990).

In the preceding paper we showed that sperm nuclei added to extracts that undergo an interphase period before entering mitosis assemble spindles that do contain morphological kinetochores and undergo at least some degree of congression to form a metaphase plate (Sawin and Mitchison, 1990). Poleward flux also occurs in these spindles, indicating that our observations of flux are not an artifact of the particular spindle assembly pathway used in the majority of our experiments. We have not yet determined whether kinetochore fibers flux in vitro; while we have not yet observed any movement suggestive of kinetochore microtubule flux (data not shown), this may reflect the difficulty of resolving poleward kinetochore microtubule flux from flux of other stable microtubules (see below).

Rates of Microtubule Turnover and Classes of Dynamic Microtubules

By varying the illumination during photoactivation experiments we found that we could observe poleward flux under condition of negligible photobleaching. Because loss of fluorescence therefore corresponds to microtubule turnover, we were able to estimate the average microtubule half-life in spindles assembled in vitro to be 75–100 s. More accurate determinations of microtubule turnover, under both normal and experimental conditions, will be possible with direct-digital fluorescence imaging and a cooled charge-coupled device (Gorbsky and Borisy, 1989). While much of the loss of fluorescence is presumably due to dynamic instability-type subunit exchange initiated at individual microtubule plus ends, we have not determined the relative contribution of loss at minus ends not attached to poles. Loss of signal at minus ends could be due either to subunit exchange at free ends, or perhaps more likely, to the photoactivated mark "running off" microtubule minus ends, the distribution of which has not yet been determined in spindles assembled in vitro. We also note here that this half-life is over an order of magnitude greater than that observed for single microtubules in mitotic extracts in vitro (Belmont et al., 1990); we have discussed the reasons for stabilization in the previous paper (Sawin and Mitchison, 1990).

Do microtubules that flux in vitro represent a special subclass of stable microtubules? Profiles of fluorescence after photoactivation suggest that both poleward flux and loss of fluorescence occur primarily if not exclusively in a single class of microtubules. We cannot rule out the existence of small (<10%) subpopulations of microtubules with different kinetic behavior. As we have noted, photoactivated fluorescence moves towards spindle poles as a coherent front, usually not resolvable into discrete bundles, and leaves no stationary fluorescent signal behind. The temporal resolution of our microscope system should be able to detect a stationary phase of even rapidly turning over microtubules, provided their half-lives are greater than the time required for free uncaged tubulin dimer to diffuse out of the spindle. Subject to the caveats given above concerning fluorescence quantitation, our results suggest that poleward microtubule flux may be a general property of any microtubule in the spindle that is stable long enough to be subject to the forces driving flux, and that microtubules in spindles assembled in vitro tend to be more stable than those spindles studied in vivo to date. The half-life of microtubules in spindles assembled in vitro is apparently greater than the 10–30 s half-lives observed in spindles in vivo using photoactivation or photobleaching techniques at physiological temperatures (Gorbsky and Borisy, 1989; Mitchison, 1989; Salmon et al., 1984*a*; Saxton et al., 1984), with the possible exception of newt lung epithelial cells (Wadsworth and Salmon, 1986). The prevalence of bar-splitting in vitro and its absence in vivo suggest greater antiparallel microtubule overlap and/or an increased midzone in vitro, and we have suggested that this may be the result of enhanced antiparallel microtubule interactions (Sawin and Mitchison, 1990). Determining whether the longer half-life of microtubules in spindles assembled in vitro is a peculiarity of amphibian cells or an artifact of extracts in vitro will require a study of poleward flux in vivo, in *Xenopus* egg and/or embryonic spindles.

Evidence for poleward flux from photoactivation is still at odds with data obtained from photobleaching experiments (Gorbsky and Borisy, 1989; Salmon et al., 1984*a*; Saxton et al., 1984; Wadsworth and Salmon, 1986), although differences might be explained by signal-to-noise problems inherent in following a small population of stable, photobleached, moving microtubules against a background of dynamic, recovering, stationary microtubules (Mitchison, 1989). In vitro, poleward flux appears to involve a more significant fraction of spindle microtubules than it does in vivo, in spindles much larger than those in tissue culture cells. Because of these differences, photoactivation experiments in vitro are relatively easy to perform. It will be interesting to see if poleward flux can be observed in this model system by photobleaching techniques.

Evidence for a Plus-end-directed Motor

Poleward flux was not inhibited by concentrations of vanadate up to 150 μM but was completely blocked by 1.7 mM AMP-PNP under conditions that affected spindle organization minimally. The pharmacology of poleward flux, in conjunction with its direction (microtubule minus ends lead, so motility is considered "plus-end directed"), are consistent with poleward flux being driven by a plus-end directed microtubule motor similar to kinesin (Cohn et al., 1989; Vale, 1987; Yang et al., 1989). In addition, the stabilization of microtubule turnover that we observed after addition of AMP-PNP might be due in part to the induction of a rigor state in such a motor (Meluh and Rose, 1990; Vale et al., 1985, but see Bershadsky and Gelfand, 1981). However, because of the nonspecificity of ATPase inhibitors and the pleiotropy of their effects in complex systems (Lee, 1989; Spurck and Pickett-Heaps, 1987), it is difficult to interpret these results simply. For example, if there were no motor and flux were driven purely by microtubule treadmilling (see below), AMP-PNP might cause a rigor state interaction between vesicle-bound motors and spindle microtubules, thereby blocking poleward flux, even though the motors might not actually drive it. Because of the nonspecific effects of inhibitors on spindle structure, we were not able to evaluate the effects of many analogues in detail; we suspect that this depends on the ability of inhibitors to compete with endogenous ATP in extracts. It will be interesting to see if poleward flux can occur under conditions where the ATP concentration can be more tightly controlled.

Nevertheless, there are additional reasons beyond our inhibitor data to think that poleward flux may be driven by a microtubule motor. Microtubule treadmilling, an intrinsic behavior of microtubules inferred from experiments with microtubule protein in vitro (Margolis and Wilson, 1978), has been proposed as a mechanism for generating force in the spindle in the absence of motor ATPases (Margolis and Wilson, 1981). However, both calculated and directly-observed rates of treadmilling in vitro are ~0.6–3 μm/h (Bergen and Borisy, 1980; Hotani and Horio, 1988; Margolis and Wilson, 1978; Rothwell et al., 1985), nearly two orders of magnitude lower than the rate of poleward flux in vitro. For this reason we doubt that the intrinsic behavior of microtubule treadmilling alone can provide the force to drive poleward flux. Furthermore, having pointed out the similarities between a postulated flux motor and kinesin, we note that a number of kinesin homologues with mitotic functions have recently been identified by genetic methods (Endow et al., 1990; Enos and Morris, 1990; McDonald and Goldstein, 1990; Meluh and Rose, 1990). We suspect that similar proteins may be driving poleward flux in the spindle; perhaps specific inhibition of flux with antibodies against motor proteins will be possible in the future.

Sites of Motors: Implications for Spindle Movements

Having observed poleward microtubule flux both in vivo and in vitro, what can we say about its function during mitosis? In metaphase and prometaphase, the forces driving poleward flux may be responsible for chromosome congression and/or maintenance of chromosome alignment (Mitchison et al., 1986; Nicklas et al., 1982; Oestergren, 1951). However, the relative speed of poleward flux in metaphase tissue culture cells (0.4–0.6 μm/min in PtK2 and LLC-PK1 cells) would seem to preclude the forces driving poleward flux from having a primary role in either anaphase A or anaphase B movements, both of which occur typically at rates of 1–2 μm/min in these cells (Brinkley and Cartwright, 1971; Mitchison, 1989; Saxton and McIntosh, 1987). One of the more striking aspects of poleward flux in vitro is its relatively rapid rate, ~3 μm/min, fast enough for flux to be involved in and perhaps principally responsible for anaphase movements in many systems. Mechanistically, poleward microtubule flux in the steady-state metaphase spindle requires precise coordination of the three essential components of flux: polymerization at microtubule plus ends, depolymerization at minus ends, and microtubule movement, with minus ends leading (Mitchison and Sawin, 1990). We have previously discussed briefly how one of the three components of flux might be uncoupled from the other two to affect either anaphase chromosome movement or spindle elongation during either anaphase or prometaphase (Mitchison and Sawin, 1990); we consider below prospective sites of flux motors and how they may relate to the function of poleward flux in spindle movements.

Mitotic Poles (Fig. 11 A). A spindle flux motor localized to or near the centrosome would entail that microtubule flux in each of half of the spindle function independently, with the centrosome drawing in microtubules; in addition, fluxing microtubules would have to be continuous within the spindle all the way back to mitotic poles. If assembly were blocked specifically at microtubule plus ends attached to kinetochores while disassembly at minus ends and a flux motor were allowed to persist, the forces driving poleward flux at metaphase could be harnessed to move chromosomes poleward in anaphase (Mitchison and Sawin, 1990). Although this is unlikely to be the primary motor for chromosome movement in mitosis (Gorbsky et al., 1988; Nicklas, 1989), such "traction fiber" movements, in concert with mechanisms involving depolymerization of microtubule ends at the kinetochore, could nevertheless contribute to the segregation of chromosomes in some systems. It is difficult to envision, however, how motors localized to centrosomes could participate directly in anaphase spindle elongation.

Antiparallel Microtubules (Fig. 11 B). In contrast, if motors driving microtubule flux were localized to and cross-bridged antiparallel microtubules, poleward flux in the spindle would consist of two half-spindles sliding directly against one another. As such, cross-bridging motors (Meluh and Rose, 1990; Shpetner and Vallee, 1989) might account for antiparallel microtubule interactions and bundling in the

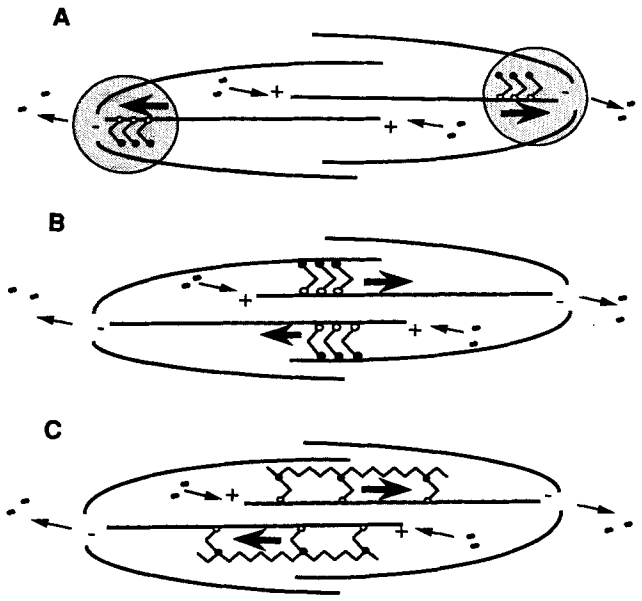

Figure 11. Potential sites for motors driving poleward microtubule flux. Each of the two half-spindles is represented by three microtubules (*heavy lines*); for purposes of clarity, chromatin has been omitted, and in each half-spindle only one microtubule is shown fluxing, in the direction of the large arrow. Subunit dimers (*figure-eights*) incorporate at plus ends and dissociate at minus ends (*small arrows*). Motors (*cocked elbows*) are drawn with one motor domain (*open circles*) and one "localization domain" (*closed circles*), although other possibilities exist (e.g., two motor domains, under the scenario in *B*). (*A*) Motors localized to the centrosome (*large circles*). (*B*) Motors localized to antiparallel microtubules. (*C*) Motors localized to a "spindle matrix" (*zig-zags*). See text for further details.

central spindle (Euteneuer et al., 1982; Euteneuer and McIntosh, 1980; McDonald et al., 1979). Furthermore, if depolymerization of microtubule minus ends at poles were blocked while assembly at plus ends and motors continued to operate, spindle elongation would ensue (Mitchison and Sawin, 1990); this would provide the force not only for spindle elongation in anaphase B (Masuda et al., 1988; Saxton and McIntosh, 1987) but also spindle expansion during prometaphase (Hogan and Cande, 1990). Experiments with individual half-spindles assembled in vitro (Sawin and Mitchison, 1990) may allow us to determine whether antiparallel microtubules are specifically required for poleward microtubule flux.

A Spindle Matrix (Fig. 11 C). Because antiparallel microtubules are unlikely to be specifically involved in the poleward flux of kinetochore microtubules in vivo (Mitchison, 1989; Mitchison et al., 1986), we believe that a microtubule cross-bridging model of poleward flux may not account for all manifestations of poleward microtubule flux. We note that motors embedded within a spindle matrix (Leslie et al., 1987) could also drive poleward flux. In this case, forces generating movement would involve two half-spindles sliding not against each other but rather against a structural matrix, that would itself be dynamic to a certain extent. A spindle-matrix motor could account for anaphase A chromosome movements, as described above, and/or metaphase chromosome alignment, consistent with force per unit length models (Nicklas et al., 1982; Oestergren, 1951). Interestingly, a spindle-matrix motor could also be envisioned as driving anaphase B spindle movements, as described above, without invoking specific antiparallel microtubule interactions. Finally, we should note that it is theoretically possible that a flux motor might be also localized to chromatin, perhaps also functioning as the force generator of astral exclusion (Rieder et al., 1986; Sawin and Mitchison, 1990); however, given our observations concerning the role of chromatin in poleward flux, we consider this unlikely.

In spite of numerous models involving motors in mitosis (see, for example, Leslie et al., 1987; Margolis and Wilson, 1981; McIntosh et al., 1969), it is still unclear why poleward microtubule flux should exist at all in the spindle. However, the simple models for mitosis derived from poleward flux are interesting in that if the motors driving poleward flux are the same as those that direct anaphase/prometaphase movements, they must already be "running" when the spindle is at steady state, i.e., when we make our observations. This offers the possibility that spindle movements might be regulated not by switching on motors per se, but rather by engaging a discrete, localized "clutch" for force transduction, the kinetochore in anaphase A, and/or the centrosome in prometaphase/anaphase B. The demonstration here of poleward flux at rates that are similar to rates of anaphase movements is intriguing; addressing in detail the role of flux in anaphase will require further experiments on anaphase spindles with similarly rapid flux rates. Having an in vitro system for poleward flux that is open to biochemical analysis should help us to understand the mechanism and/or regulation of poleward flux on a molecular level. This in turn should contribute to our understanding of the physiological function of poleward microtubule flux in mitosis.

We are grateful to Tony Hyman for his contributions towards assembling the microscope system used in these experiments. We thank Richard Durbin for writing key routines and for introducing us to C programming, Swati Mujumdar and Alan Waggoner for providing us with CY5, and Mr. Hohner's slaughterhouse (San Leandro, CA) for most excellent brains. We also thank Ron Vale for a critical reading of the manuscript.

This work was supported by National Institutes of Health grant GM39565 and by fellowships from the Chicago Community Trust, the David and Lucile Packard Foundation and the National Science Foundation. T. Mitchison is a Searle Scholar and a Packard Fellow. K. Sawin is a National Science Foundation predoctoral fellow.

Received for publication 15 August 1990 and in revised form 22 October 1990.

References

Belmont, L. D., A.A. Hyman, K. E. Sawin, and T. J. Mitchison. 1990. Real-time visualization of cell cycle dependent changes in microtubule dynamics in cytoplasmic extracts. *Cell.* 62:579–589.

Bergen, L. G., and G. G. Borisy. 1980. Head-to-tail polymerization of microtubules in vitro. *J. Cell Biol.* 84:141–150.

Bershadsky, A. D., and V.I. Gelfand. 1991. ATP-dependent regulation of cytoplasmic microtubule disassembly. *Proc. Natl. Acad. Sci. USA.* 78(6):3610–3613.

Brinkley, B. R., and J. J. Cartwright. 1971. Ultrastructural analysis of mitotic spindle elongation in mammalian cells in vitro: direct microtubule counts. *J. Cell Biol.* 50:416–431.

Cassimeris, L., S. Inoue, and E. D. Salmon. 1988. Microtubule dynamics in the chromosomal spindle fiber: analysis by fluorescence and high-resolution polarization microscopy. *Cell Motil. Cytoskeleton.* 10:185–196.

Cohn, S.A., A. L. Ingold, and J. M. Scholey. 1989. Quantitative analysis of sea urchin kinesin-driven microtubule motility. *J. Biol. Chem.* 264(8): 4290–4297.

Endow, S.A., S. Henikoff, and L. S. Niedziela. 1990. Mediation of meiotic and early mitotic chromosome segregation in Drosophila by protein related to kinesin. *Nature (Lond.)*. 345:81–83.

Enos, A. P., and N. R. Morris. 1990. Mutation of a gene that encodes a kinesin-like protein blocks nuclear division in A. nidulans. *Cell*. 60:1019–1027.

Ernst, L. A., R. K. Gupta, R. B. Mujumdar, and A. S. Waggoner. 1989. Cyanine dye labeling reagents for sulfhydryl groups. *Cytometry*. 10(1):3–10.

Euteneuer, U., and J. R. McIntosh. 1980. Polarity of midbody and phragmoplast microtubules. *J. Cell Biol.* 87:509–515.

Euteneuer, U., W. T. Jackson, and J. R. McIntosh. 1982. Polarity of spindle microtubules in Haemanthus endosperm. *J. Cell Biol.* 94:644–653.

Gorbsky, G. J., and G. G. Borisy. 1989. Microtubules of the kinetochore fiber turn over in metaphase but not in anaphase. *J. Cell Biol.* 109(2):653–662.

Gorbsky, G. J., P. J. Sammak, and G. G. Borisy. 1988. Microtubule dynamics and chromosome motion visualized in living anaphase cells. *J. Cell Biol.* 106:1185–1192.

Hamaguchi, Y., M. Toriyama, H. Sakai, and Y. Hiramoto. 1987. Redistribution of fluorescently labeled tubulin in the mitotic apparatus of sand dollar eggs and the effects of taxol. *Cell Struct. Funct.* 12:43–52.

Hogan, C. J., and W. Z. Cande. 1990. Antiparallel microtubule interactions: spindle formation and anaphase B. *Cell Motil. Cytoskeleton*. 16:99–103.

Hotani, H., and T. Horio. 1988. Dynamics of microtubules visualized by darkfield microscopy: treadmilling and dynamic instability. *Cell Motil. Cytoskeleton*. 10:229–236.

Hyman, A., D. Drechsel, D. Kellogg, S. Salser, K. Sawin, P. Steffen, L. Wordeman, and T. Mitchison. 1990. Preparation of modified tubulins. *Methods Enzymol.* In press.

Inoue, S., and H. Sato. 1967. Cell motility by labile association of molecules: the nature of mitotic spindle fibers and their role in chromosome movement. *J. Gen. Physiol.* 50:259–292.

Kirschner, M. W., and T. J. Mitchison. 1986. Beyond self assembly: from microtubules to morphogenesis. *Cell*. 45:329–342.

Lee, G. M. 1989. Characterization of mitotic motors by their relative sensitivity to AMP-PNP. *J. Cell Sci.* 94:425–441.

Leslie, R. J., R. B. Hird, L. Wilson, J. R. McIntosh, and J. M. Scholey. 1987. Kinesin is associated with a nonmicrotubule component of sea urchin mitotic spindle. *Proc. Natl. Acad. Sci. USA*. 84:2771–2775.

Lohka, M. J., and J. L. Maller. 1985. Induction of nuclear envelope breakdown, chromosome condensation, and spindle formation in cell-free extracts. *J. Cell Biol.* 101:518–523.

Margolis, R. L., and L. Wilson. 1978. Opposite end assembly and disassembly of microtubules at steady state in vitro. *Cell*. 13:1–8.

Margolis, R. L., and L. Wilson. 1981. Microtubule treadmills—possible molecular machinery. *Nature (Lond.)*. 293:705–711.

Masuda, H., K. L. McDonald, and W. Z. Cande. 1988. The mechanism of anaphase spindle elongation: uncoupling of tubulin incorporation and microtubule sliding during in vitro spindle reactivation. *J. Cell Biol.* 107: 623–633.

McDonald, H.B., and L. S. B. Goldstein. 1990. Identification and characterization of a gene encoding a kinesin-like protein in Drosophila. *Cell*. 61:991–1000.

McDonald, K. L., M. K. Edwards, and J. R. McIntosh. 1979. Cross-sectional structure of the central mitotic spindle of Diatoma vulgare. *J. Cell Biol.* 83:443–461.

McIntosh, J. R., P. K. Helpler, and D. G. Van Wie. 1969. Model for mitosis. *Nature (Lond.)*. 224:659–663.

Meluh, P. B., and M.D. Rose. 1990. KAR3, a kinesin-related gene required for yeast nuclear fusion. *Cell*. 60:1029–1041.

Mitchison, T. J. 1988. Microtubule dynamics and kinetochore function in mitosis. *Annu. Rev. Cell Biol.* 4:527–550.

Mitchison, T. J. 1989. Polewards microtubule flux in the mitotic spindle: evidence from photoactivation of fluorescence. *J. Cell Biol.* 109:637–652.

Mitchison, T. J., and M. W. Kirschner. 1984. Dynamic instability of microtubule growth. *Nature (Lond.)*. 312:237–242.

Mitchison, T. J., and M. W. Kirschner. 1985. Properties of the kinetochore in vitro. 2. Microtubule capture and ATP dependent translocation. *J. Cell Biol.* 101:767–777.

Mitchison, T. J., and K. E. Sawin. 1990. Tubulin flux in the mitotic spindle: where does it come from, where is it going? *Cell Motil. Cytoskeleton*. 16:93–98.

Mitchison, T. J., L. Evans, E. Schultze, and M. W. Kirschner. 1986. Sites of microtubule assembly and disassembly in the mitotic spindle. *Cell*. 45: 515–527.

Murray, A. W., and M. W. Kirschner. 1989. Cyclin synthesis drives the early embryonic cell cycle. *Nature (Lond.)*. 339:275–280.

Nicklas, R. B. 1989. The motor for poleward chromosome movement in anaphase is in or near the kinetochore. *J. Cell Biol.* 109(5):2245–2255.

Nicklas, R. B., D. F. Kubai, and T. S. Hays. 1982. Spindle microtubules and their mechanical associations after micromanipulation in anaphase. *J. Cell Biol.* 95:91–104.

Oestergren, G. 1951. The mechanism of coordination in bivalents and multivalents: the theory of orientation by pulling. *Hereditas*. 37:85–156.

Paschal, B. M., and R. B. Vallee. 1987. Retrograde transport by the microtubule-associated protein MAP 1C. *Nature (Lond.)*. 330(6144):181–183.

Rieder, C. L. 1981. The structure of the cold stable kinetochore fiber in metaphase PtK1 cells. *Chromosoma (Berl.)*. 84:145–158.

Rieder, C. L., E. A. Davison, L. C. W. Jensen, L. Cassimeris, and E. D. Salmon. 1986. Oscillatory movements of monooriented chromosomes and their position relative to the spindle pole result from the ejection properties of the aster and the half-spindle. *J. Cell Biol.* 103:581–591.

Rothwell, S., W. Grasser, and D. Murphy. 1985. Direct observation of microtubule treadmilling by electron microscopy. *J. Cell Biol.* 101:1637–1642.

Salmon, E. D., R. J. Leslie, W. M Karow, J. R. McIntosh, and R. J. Saxton. 1984*a*. Spindle microtubule dynamics in sea urchin embryos: analysis using fluorescence-labeled tubulin and measurements of fluorescence redistribution after laser photobleaching. *J. Cell Biol.* 99:2165–2174.

Salmon, E. D., M. McKeel, and T. Hays. 1984*b*. Rapid rate of tubulin dissociation from microtubules in the mitotic spindle in vivo measured by blocking polymerization with colchicine. *J. Cell Biol.* 99:1066–1075.

Sammak, P. J., G. J. Gorbsky, and G. G. Borisy. 1987. Microtubule dynamics in vivo: a test of mechanisms of turnover. *J. Cell Biol.* 104(3):395–405.

Sawin, K. E., and T. J. Mitchison. 1990. Mitotic spindle assembly by two different pathways in vitro. *J. Cell Biol.* 112:925–940.

Saxton, W. M., and J. R. McIntosh. 1987. Interzone microtubule behavior in late anaphase and telophase spindles. *J. Cell Biol.* 105:875–886.

Saxton, W. M., D. L. Stemple, R. J. Leslie, E. D. Salmon, M. Zavortink, and J. R. McIntosh. 1984. Tubulin dynamics in cultured mammalian cells. *J. Cell Biol.* 99:2175–2186.

Shpetner, H. S., and R. B. Vallee. 1989. Identification of dynamin, a novel mechanochemical enzyme that mediates interactions between microtubules. *Cell*. 59:421–432.

Shpetner, H. S., B. M. Paschal, and R. B. Vallee. 1988. Characterization of the microtubule-activated ATPase of brain cytoplasmic dynein (MAP 1C). *J. Cell Biol.* 107:1001–1009.

Southwick, P. L., L. A. Ernst, E. W. Tauriello, S. R. Parker, R. B. Mujumdar, S. R. Mujumdar, H. A. Clever, and A. S. Waggoner. 1990. Cyanine dye labeling reagents—carboxymethylindocyanine succinimidyl esters. *Cytometry*. 11(3):418–430.

Spurck, T. P., and J. D. Pickett-Heaps. 1987. On the mechanism of anaphase A: evidence that ATP is needed for microtubule disassembly and not generation of polewards force. *J. Cell Biol.* 105:1691–1705.

Vale, R. D. 1987. Intracellular transport using microtubule based motors. *Annu. Rev. Cell Biol.* 3:347–378.

Vale, R. D., T. S. Reese, and M.P. Sheetz. 1985. Identification of a novel force-generating protein, kinesin, involved in microtubule-based motility. *Cell*. 42:39–50.

Vigers, G. P. A., M. Coue, and J. R. McIntosh. 1988. Fluorescent microtubules break up under illumination. *J. Cell Biol.* 107:1011–1024.

Wadsworth, P., and E. D. Salmon. 1986. Analysis of the treadmilling model during metaphase of mitosis using fluorescence redistribution after photobleaching. *J. Cell Biol.* 102:1032–1038.

Walker, R. A., E. T. O'Brien, N. K. Pryer, M. F. Sobeiro, W. A. Voter, H. P. Erickson, and E. D. Salmon. 1988. Dynamic instability of individual microtubules analyzed by video light microscopy: rate constants and transition frequencies. *J. Cell Biol.* 107:1437–1448.

Yang, J. T., R. A. Laymon, and L. S. B. Goldstein. 1989. A three-domain structure of kinesin heavy chain revealed by DNA sequence and microtubule binding analyses. *Cell*. 56:879–889.